

This article may be downloaded for personal use only. Any other use requires prior permission of the author and American Physical Society.

The following article appeared in *Phys. Rev. E* 77, 036223 (March 2008) and may be found at <https://doi.org/10.1103/PhysRevE.77.036223>

Pattern formation by two precipitated species during solvent evaporation

Gerardo Lara-Cisneros,¹ Abigail Loredó-Osti,² Ricardo Femat,³ and Elías Pérez²

¹*CIEP-Facultad de Ciencias Químicas, UASLP, Manuel Nava 6, 78290 San Luis Potosí, Mexico*

²*Instituto de Física, Universidad Autónoma de San Luis Potosí, Alvaro Obregón 64, 78000 San Luis Potosí, Mexico*

³*Laboratorio de Biodinámica y Sistemas Alineales, División de Matemáticas Aplicadas, IPICYT, Camino a la Presa San José 2055, 78216, San Luis Potosí, Mexico*

(Received 15 April 2007; revised manuscript received 22 August 2007; published 27 March 2008)

We investigate the pattern formation produced by precipitated species during solvent evaporation through the numerical solution of a set of partial differential equations that account for the mechanisms of evaporation, diffusion, and precipitation. A pattern is formed because solvent evaporation provokes precipitation of species near the border of the system producing ringlike depositions from the edge to the center. Solvent evaporation is modeled as occurs with a liquid drop on a surface. The spacing between rings and its width are constant and roughly constant, respectively. Pattern formation follows the evaporation process inducing trends on pattern formation that are different to those produced by the precipitation of two species in a diffusive front (Liesegang rings). The spatial structure of rings under solvent evaporation is similar to those observed during solvent evaporation on two oppositely charged colloids and is attributable to the competition between precipitation and evaporation processes.

DOI: [10.1103/PhysRevE.77.036223](https://doi.org/10.1103/PhysRevE.77.036223)

PACS number(s): 05.45.-a, 47.54.-r, 47.20.Ma

I. INTRODUCTION

Microscopic particles in a drop of suspension placed on a surface remain near the contact line between the drop and surface after the solvent evaporates because evaporation occurs close to this line [1]. A typical example of this effect is the ringlike stains left by a spilled coffee drop after its evaporation. Convective flow inside the drop during evaporation, from the center to the edge, has been identified for a large variety of surfaces and solvents as the main driving force for the particle deposition [1,2]. Deposition is modulated by the geometrical constraints imposed by the contact angle and the deposition surface [3] as well as by the electrical charge between the particles and the surface [4]. Furthermore, controlled experiments have shown that particle suspensions can produce or induce pattern formation from the competition between liquid pinning and dewetting during evaporation. A pattern is formed by precipitated particles depending on distinct factors, such as particle size and concentration, solid packing, arch-shaped, radial lines, or disordered zones [5].

Although pattern formation has been studied on diffusion-reaction systems since Turing seminal work [6,7], this has not been the case for patterns formed under evaporation. The called Liesegang patterns represent typical examples close to the patterns produced by evaporation since the precipitated species are at the border of the systems. Liesegang experimental setup consists of a chemical reactant dissolved in a gel matrix and a second reactant that diffuses into the gel [8–11]. Liesegang patterns are formed by precipitates that form either bands [one dimensional (1D)] or rings [two dimensional (2D)] of material [8–15]. The bandlike structures (1D) obey temporal and spatial laws that establish the following [12]: (i) The position of the n th band (X_n) is proportional to $\sqrt{t_n}$, where t_n is the time elapsed until the appearance of the n band, (ii) for a large n , the ratio of the positions of two consecutive bands approaches a constant value, then

$(X_{n+1}/X_n) \rightarrow 1+p$, with p a positively spacing coefficient comprising between $0.05 < p < 0.4$, and (iii) the bandwidth (W_n) is proportional to X_n . In regard to ringlike structures, similar laws are expected but with the geometric effect superposed [11]. While the first law is a direct consequence of that the diffusion controls the Liesegang patterns, the second and third laws do not have a simple interpretation. However, models based on the Ostwald's supersaturation theory have been able to reproduce them [12].

Although patterns produced by evaporation may also obey distinct laws that Liesegang rings, these have not been fully stated yet. Some differences have been found with respect to well-stated pattern formation. For example, contrarily to usual 2D Liesegang rings, rings formed by evaporation appear from edge to center. That is, under evaporation, particle deposition departs with a transient zone, followed by a zone where the rings are well defined and, finishing with a zone, close to the center, where the particles are disordered [4,5]. For the case of positive particles on hydrophilic negatively charged surfaces, experiments have shown that $\Delta X_n = X_{n+1} - X_n$ is wide at the beginning and decreases gradually to a constant. At the same time, W_n increases until it reaches a maximum and then it decreases gradually before arriving at the disordered zone, both ΔX_n and W_n quantities measured from the edge to the center [4].

Theoretical and experimental studies have been performed on pattern formation by evaporation of a drop of colloidal suspension on a substrate [1,2,16–21]. Stripe pattern formation is mostly attributed to the stick-slip motion on the contact line caused by the competition processes between the particle flow induced by the evaporation (i.e., the convective process) and the drop shrinkage; this last process is due to surface tension force in the plane of the substrate [1,2,16,17,20,21,23]. Other reports include regular pattern formation by drop evaporation from restricted geometries [18,19]. However, as mentioned above, pattern formation by evaporation of a drop of colloidal suspension is not completely elucidated. As a matter of fact, competition between

evaporation and precipitation is an open issue. Thus, the statement of models accounting effects of this phenomenon is our interest.

In the present work, we investigate the pattern formation by two diffusive species under both precipitation and evaporation. The system is such that precipitate follows the supersaturation theory [12], and the solvent evaporates as a liquid drop on a surface. This approach yields a set of partial differential equations (PDEs) that were solved numerically producing simulated rings. The methodology has shown to be powerful in the study of Liesegang structures [13–15]. The spatial distribution of rings is derived numerically and compared with those obtained experimentally for precipitation of charged particles on a surface during solvent evaporation. Conclusions of specific rules are discussed. The rest of paper is organized as follows. Section II includes the experimental results that motivated this work. Section III presents the numerical model and the technique to resolve the PDE system. Section IV presents the results derived and their discussion. Finally, Sec. V presents the conclusions.

II. EXPERIMENT

The experimental system consisted of positively and negatively charged colloidal particles suspended in water. Colloidal particles were made of poly(styrene) by surfactant-free emulsion polymerization using 2-2'-Azobis (2-methylpropionamide) dihydrochloride and persulfate of potassium as initiators for positive and negative particles, respectively. Both positive and negative particles were synthesized using 150 ml of water, 16 ml of styrene, and 0.04 g of initiator. Synthesis was carried out at 70 °C, and stirred at 750 rpm during 24 h. Details on this polymerization are given elsewhere [22]. Positive particles were 645 nm (with a polydispersity lesser than 10%) while negative particles were 583 nm (and polydispersity around 4%). The electrical charge of the particles was verified by ζ potential measurements. The experimental setup is simple. A micropipette is fixed at a laboratory stand 1 cm above a leveled microscope slide whose temperature was set at 70 °C by a hot plate. 150 μ l, at 0.01% in solid fraction of particles, were then gently dripped onto the glass surface. Following the dripping, the slide was kept in place until complete water evaporation; it takes only a few minutes. At the end, the images of the particle deposition were captured using a microscopy Olympus CX31 with an amplification of 4 \times .

Depending on the electrical charge of particles, two different behaviors were observed: Positive particles are precipitated onto a negatively charged surface, while negative particles precipitated until almost total solvent evaporation. In both cases, the precipitated material formed a big deposition of particles on the microscope slide, as shown in Figs. 1(a) and 1(b). Therefore, the pattern formation by suspensions of particles of the same electrical sign is not present at the present experimental conditions. The pattern formation occurs as a mixture of positive and negative particles in suspension (50%–50% in volume) are deposited on the glass surface [see Fig. 2(a)]. The pattern is formed from drop edge toward its center. During the pattern formation, particles are

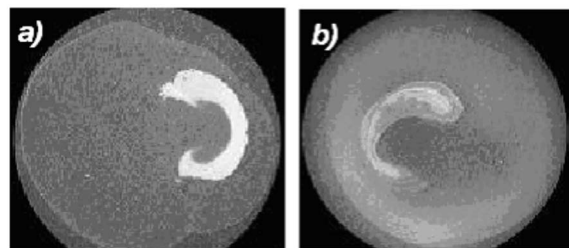


FIG. 1. Deposition of colloidal particles on a negatively charged surface. (a) Positive particles; (b) negative particles in suspension. In both cases, patterns are not formed. Samples of 1×1 cm².

fixed on the surface after the particle precipitation. The pattern in Fig. 2(a) is driven by a different force, such as surface tension, drop pinning, and evaporation, as mentioned above. On this step, we model the pattern formation including effects due to diffusion, precipitation, and evaporation processes. Figure 2(b) shows a simulated pattern generated by this simulation, which is discussed after the presentation of the numerical simulation.

III. NUMERICAL SIMULATION

In this section we state the set of the partial differential equations to model the pattern formation modulated by an evaporation process. We focused on evaporation that occurs in a sessile drop, which is described by two parameters: The drop radius (R) and the contact angle (θ_c). When evaporation occurs from the edge, evaporated solvent flux $J_s(r, \theta_c)$ (outside the drop) and convective velocity $v(r, t)$ (inside the drop) as function of r coordinate, are given by [2]

$$J_s(r, \theta_c) = J_0[1 - (r/R)^2]^{-\lambda(\theta_c)}, \quad (1)$$

$$v(r, \theta_c) = -\frac{1}{\rho h r} \int_0^r s J_s(s, \theta_c) ds, \quad (2)$$

where $\lambda(\theta_c) = \pi - 2\theta_c / 2\pi - 2\theta_c$, with $\theta_c \in [0, \pi/2]$, provides the dependence with the contact angle, and J_0 represents the intensity of the flux of evaporation in the center of the drop, h is the drop thickness, and ρ is the density of the solvent. Pattern formation always occurs for a θ_c sufficiently small to

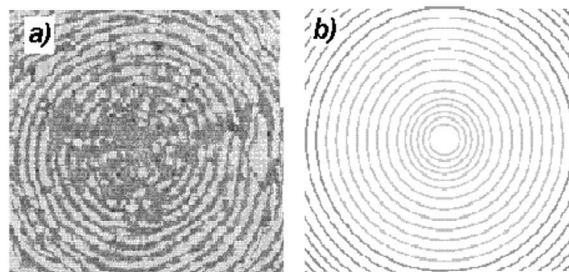


FIG. 2. (a) An experimental pattern formed by oppositely charged colloidal particles in suspension after water evaporation. Sample of 1×1.15 cm². (b) A simulated pattern obtained by simulation using as precipitation parameter $\beta=500$, and evaporation parameter $\gamma=4.0$ (b).

trap the particles by the surface of deposition and free surface of liquid-air interface [4]. In this case, $\lambda \approx 1/2$ is an approach to the angular function.

The precipitates were assumed to be formed by a local reaction $a(r,t)+b(r,t) \rightarrow c(r,t)$, without intermediate product, where a and b are concentration of reactants and c is precipitated concentration. Although concentration of reactants decreases by the reaction, they are increased by the solvent evaporation. Thus, a competition between precipitation and evaporation is always present. For the specie a , this effect is given by

$$J_e(a,r) = aJ_s(r) - \frac{1}{r} \frac{\partial a}{\partial r} \int_0^r rJ_s(s)ds = \frac{a}{r} \frac{\partial}{\partial r}[rv(r)] + v(r) \frac{\partial a}{\partial r}, \quad (3)$$

where the first term on the right-hand side of (3) denotes the local contribution of the evaporation flux while the second term comes from the dependence of a with convective transport inside the drop. The identity is an alternative form to write this contribution in terms of $v(r)$ using Eq. (2). Note that $J_e(a,r)$ have two divergences: At $r=R$ and at $r=0$; due to $J_s(r)$ and $v(r)$ divergences, respectively.

Supersaturation theory is assumed to describe the precipitation process [15]; that is, the precipitation term is given by

$$\delta(ab,K,L) = \begin{cases} \kappa \delta_p \Theta(ab-K) & \text{if } c=0, \\ \kappa \delta_p \Theta(ab-L) & \text{if } c>0, \end{cases} \quad (4)$$

where κ is the rate constant of the precipitation reaction, based on Ostwald's supersaturation theory [13]. $\Theta: \mathbb{R} \rightarrow \{0,1\}$ is a step function and K and L define the product threshold of the nucleation and precipitation, respectively. δ_p is the increment of the precipitation product, and is calculated from the equation $(a-\delta_p)(b-\delta_p)=L$.

A mass balance for two reactant species and precipitate yields to a set of PDEs. Mass balance takes into account diffusion, precipitation, and convection for the reactants and only the precipitation for the precipitate. Thus, we have the following model in dimensionless variables $\xi=r/R$ and $\tau=D_a t/R^2$:

$$\frac{\partial a}{\partial \tau} = \frac{\partial^2 a}{\partial \xi^2} + \frac{1}{\xi} \frac{\partial a}{\partial \xi} - \beta \delta(ab) + \gamma j_e(a,\xi), \quad (5)$$

$$\frac{\partial b}{\partial \tau} = \phi \left(\frac{\partial^2 b}{\partial \xi^2} + \frac{1}{\xi} \frac{\partial b}{\partial \xi} \right) - \beta \delta(ab) + \gamma j_e(b,\xi), \quad (6)$$

$$\frac{\partial c}{\partial \tau} = \beta \delta(ab), \quad (7)$$

with the dimensionless parameters

$$\phi = \frac{D_b}{D_a}, \quad \beta = \frac{R^2 \kappa}{D_a}, \quad \gamma = \frac{R^2 J_0}{\rho h D_a}, \quad (8)$$

where $j_e(a,r)$ and $j_e(b,r)$ are the corresponding dimensionless terms of $J_e(a,r)$ and $J_e(b,r)$. Equation (7) does not contain the diffusive term or the convective one; which implies

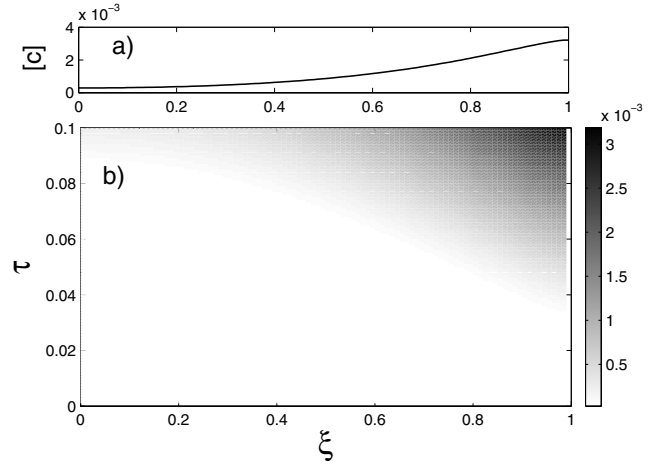


FIG. 3. Precipitate deposition for $\beta=1$ and $\gamma=1$ (a) The final profile of the precipitate. (b) Temporal and spatial evolution of the front. Only the deposition close to the border is present.

that the precipitate is fixed after precipitation, as experimentally observed.

Standard boundary conditions were established assuming no mass flux at the border, and considering radial symmetry, at $\xi=0$ and $\xi=1$, they are

$$\frac{\partial a}{\partial \xi} = 0, \quad \frac{\partial b}{\partial \xi} = 0. \quad (9)$$

Note that boundary conditions do not take into account more complete conditions, such as contact line pinning, and then the model is limited to these conditions. Equations (5)–(7) were solved reducing the PDEs into a set of ordinary differential equations after a spatial division in an equidistant 1D grid [24]. The set of ODE were integrated in time using a fourth-order Runge-Kutta method.

In this study, diffusion coefficients were assumed constant, with $\phi=1$, and β and γ were taken to have the following values: $\beta=1, 10, 50, 100, 500, 1000$ and $\gamma=0.5, 1, 2, 3, 4$. Homogeneous initial conditions were assumed with $a(\xi,0)=b(\xi,0)=0.3$ and $c(\xi,0)=0$. The grid spacing and time step were chosen as $\Delta\xi=0.01$ and $\Delta\tau=10^{-5}$, with $\xi \in [0,1]$ and $\tau \in [0, \tau_{\max}]$. τ_{\max} was approximated from the diffusion coefficient of the colloidal particles and typical size of patterns (few millimeters), obtaining a value of $\tau_{\max}=0.1$ which was sufficient to establish a developed profile.

IV. RESULTS AND DISCUSSION

In order to investigate effects of competition between precipitation and evaporation processes on the pattern formation, the patterns were generated from Eqs. (5)–(7) as described above. The origin of space coordinate is arbitrarily located, without loss of generality, in the center of the pattern [15]. Two contrasting examples are shown in Figs. 3 and 4. In Fig. 3 only the precipitated ring is formed at the border (close to $\xi=1.0$). This occurs for $\beta=1$ and $\gamma=1$, and means that this ring is in general dominant due to divergence of the convective term, see Eq. (3). The steady-state (precipitation)

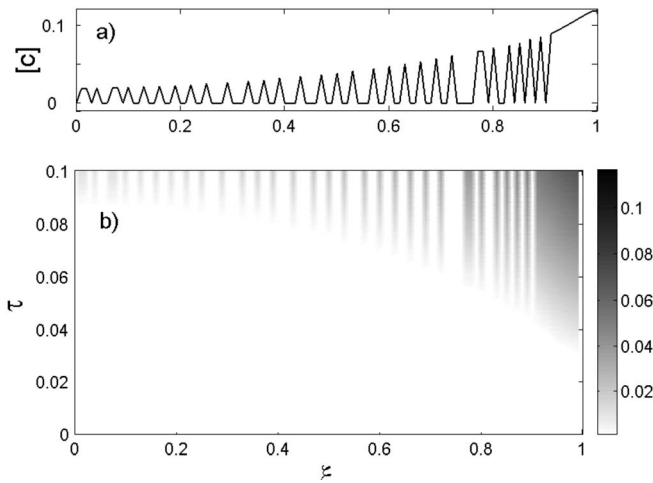


FIG. 4. Pattern formation for $\beta=100$ and $\gamma=1$. (a) The final profile of the precipitate. (b) Temporal and spatial evolution of the front.

profile is presented at the top in Fig. 3, where a monotonic decreasing precipitation toward the center is shown. The pattern in Fig. 4 corresponds to a second case where $\beta=100$ and $\gamma=1$. In this case, the precipitate forms a series of rings as a function of time at a fixed position that represents our main concern.

Examples in a wide interval for both β and γ values are shown in Figs. 5 and 6. The bands in both Figs. 5 and 6 correspond to deposition along a radial coordinate. In Fig. 5, $\gamma=1$ and β take the following values, respectively, 10, 50, 100, 500, and 1000. Note that only the precipitate (one band) at the edge is formed for $\gamma=1$ and $\beta=10$, as shown in Fig. 5(a). As the β increases, the precipitation is stronger (i.e., precipitation is more important whereas evaporation holds constant). Hence, rings appear [see Fig. 6(b)]. This shows that the precipitation process is important for pattern formation. However, the number of rings is not increased with respect to β values, as shown in Figs. 5(c)–5(e). As matter of fact, the number of rings decreases after $\beta=100$. This is attributable to the competition between the evaporation and

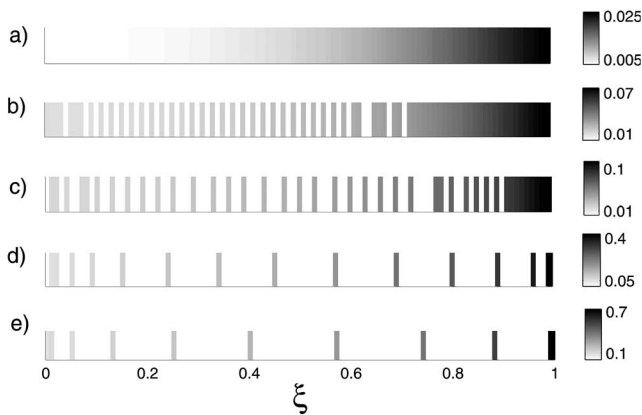


FIG. 5. Rings formation at different precipitation conditions with $\gamma=1$: (a) $\beta=10$; (b) $\beta=50$; (c) $\beta=100$; (d) $\beta=500$; (e) $\beta=1000$.

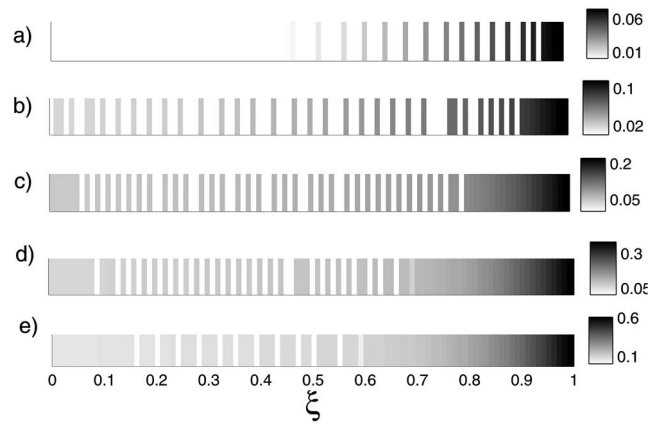


FIG. 6. Rings formation at different evaporation conditions with $\beta=100$: (a) $\gamma=0.5$; (b) $\gamma=1$; (c) $\gamma=2$; (d) $\gamma=3$; (e) $\gamma=4$.

precipitation processes. In Fig. 6 the β value is fixed to 100 to assure pattern formation, whereas γ is varied from 0.5 to 4. In this case, the number of rings increases as shown in Figs. 7(a)–7(c). Thereafter, decreasing of its number with γ values larger than 3; indicating the existence of maximum formation of precipitate rings. High values of the γ parameter also inhibit a great number of rings.

We observed that only under a suitable combination of β and γ are the patterns formed. Figure 7 shows the number of precipitated rings, as contour curves, for the overall region explored (where the two dotted lines are drawn to indicate the cases shown in Figs. 5 and 6). In general, these patterns are obtained for low- γ and high- β values. This means that a precipitation is required in order to obtain patterns but number of rings is defined by the parameter values. Therefore, that existence of a maximum of rings indicates a coupling between the precipitation and evaporation processes. In all of the above-presented patterns the precipitated deposition, computed by a mass integration of precipitate around the ring position, does not exhibit a maximum. Hence, this maxi-

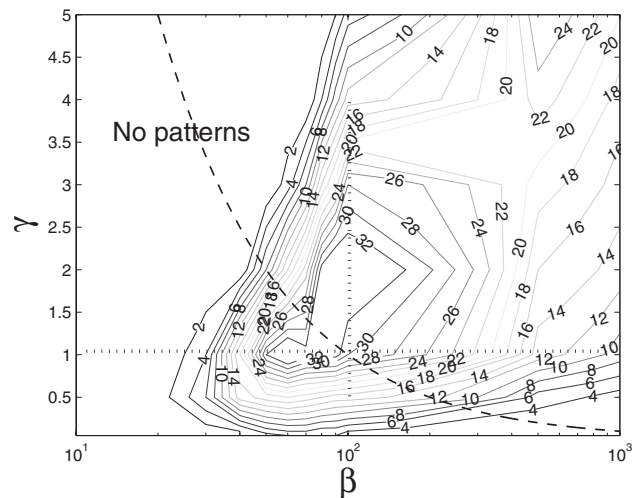


FIG. 7. Level curves of the number of rings formed with the parameters of simulation (β, γ). Dotted lines represent the axes explored in Figs. 5 and 6. Dashed line represents an hyperbola with the particle diffusion constant.

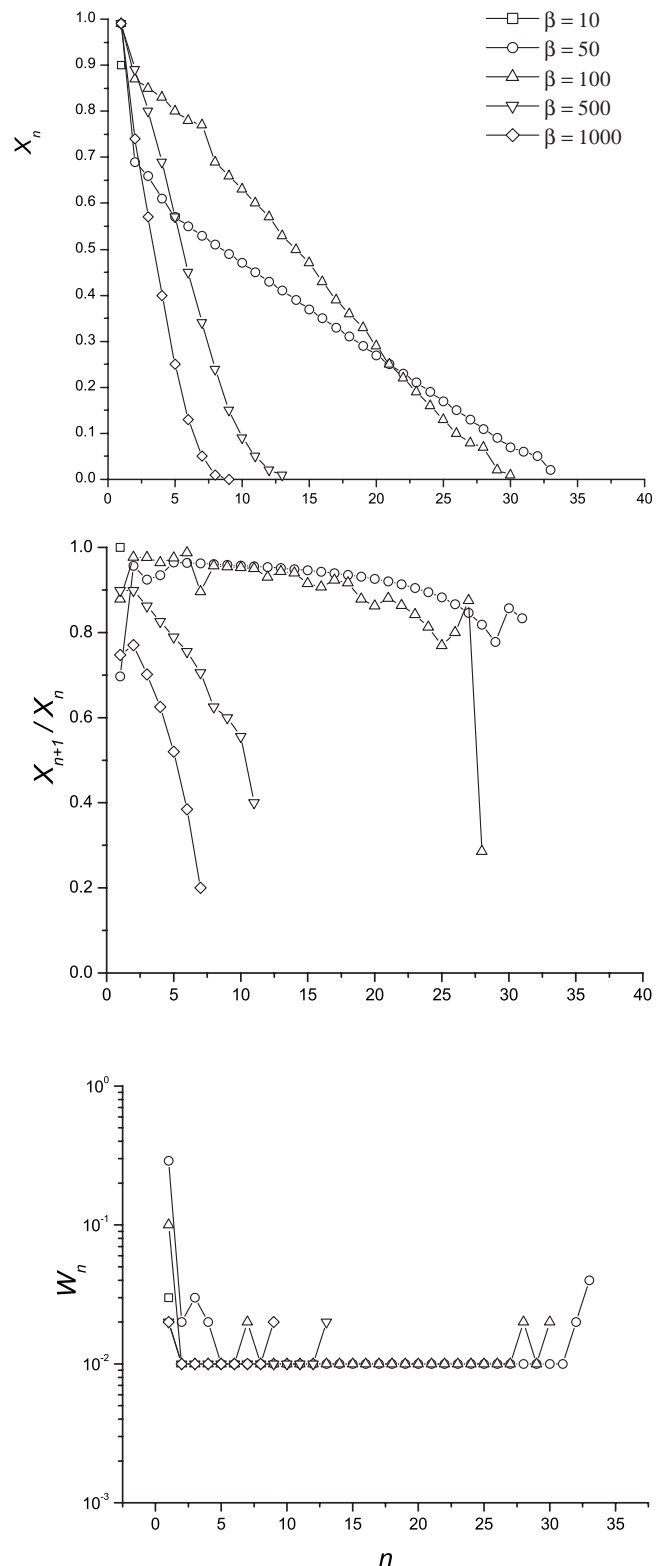
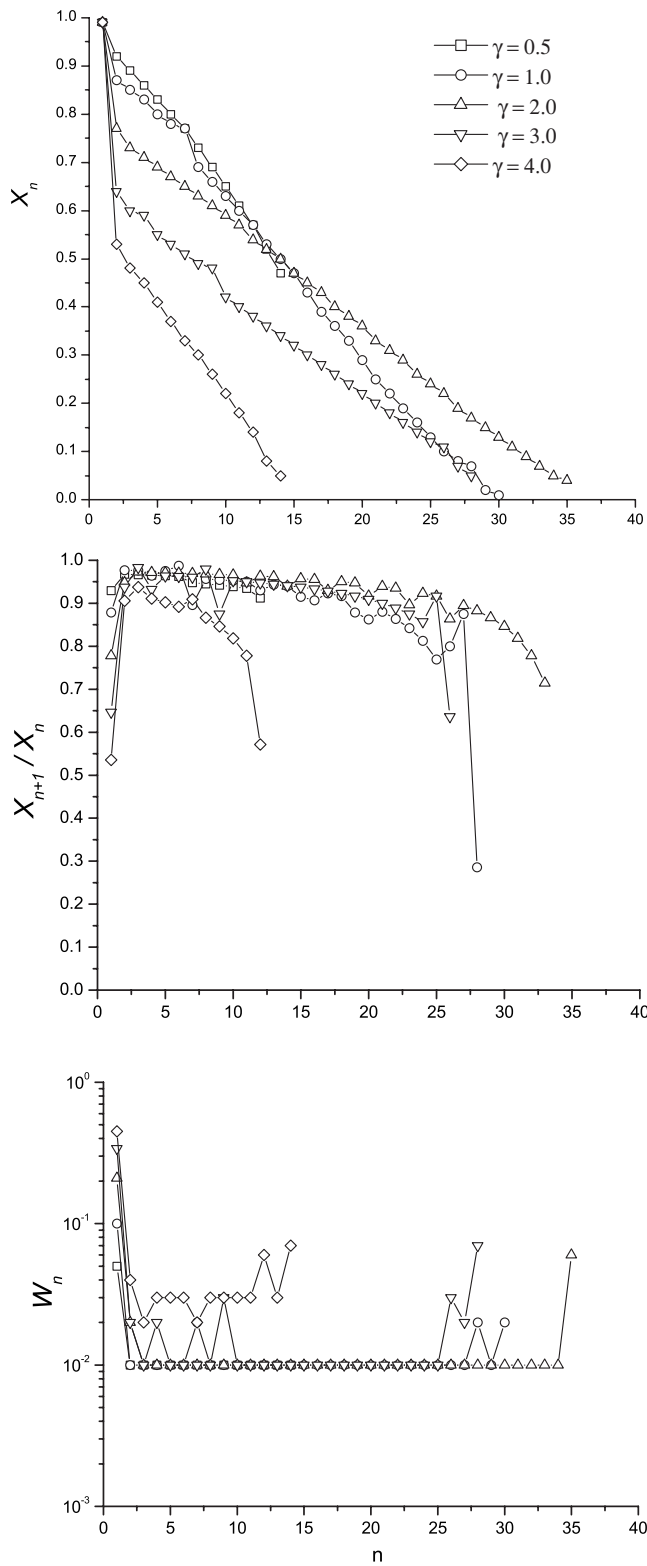


FIG. 8. X_n , X_{n+1}/X_n , W_n at different evaporation parameters with $\beta=100$.

FIG. 9. X_n , X_{n+1}/X_n , W_n at different precipitation parameters with $\gamma=1$.

mum is not characteristic of a resonant effect.

Figures 8 and 9 depict X_n , X_{n+1}/X_n , and W_n derived from a spatial analysis of these simulations. The space analysis shows that the deposition in the center is negligible because

it is too thick due to the divergent term at $\xi=0$ [see Eqs. (2) and (3)]. X_n has a monotonic decreasing form attributable to restriction in precipitation in the center of the drop. Also note that there is an important decreasing from the first point and

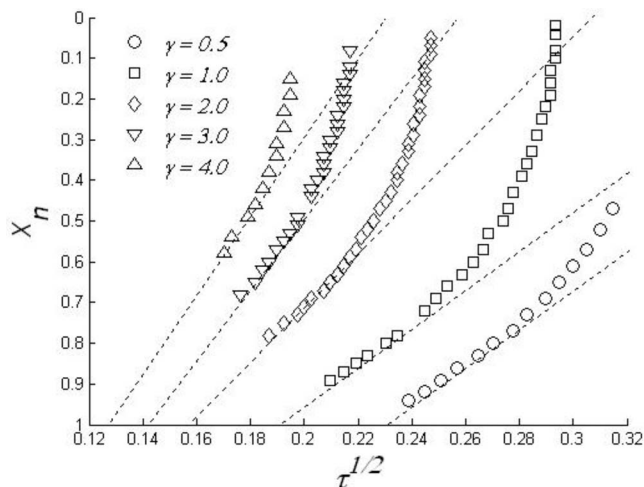


FIG. 10. Different dynamic regimes are defined with the evaporation parameter at $\beta=100$.

the second one that is stronger for high values of β and γ because the first ring is thicker in these cases. X_{n+1}/X_n follows a lightly decreasing behavior with the exception of the values near the origin and the edge ($\xi=0$ and $\xi=1$), where the change is stronger, indicating that the first rings and the last ones are in general closer to each other. It is again more evident for high values of β and γ . X_{n+1}/X_n is roughly constant in the middle of the pattern and spacing coefficient (p) can be calculated; which can be related to the mechanism of precipitation. Otherwise, W_n is effectively constant in that region far from the center and the edge of the drop, indicating a very well-defined process of precipitation.

Dependence of position X_n versus $\tau_n^{1/2}$ is shown in Figs. 10 and 11. This provides us with complementary information. In both cases, the straight lines represent the diffusion associated to these parameters, which evidently is not followed by these patterns. There is also a divergence for the last rings (near the center), which are also characteristic of the evaporation process close to the drop center. Indeed, in Fig. 10, precipitation parameter (β) is fixed to 100 while the evaporation parameter (γ) is varied from 0.5 to 5. In this case, different tendencies during the pattern formation are stated in contrast to the case in Fig. 11, where $\gamma=1$ and β is varied from 50 to 1000. We observe that a unique tendency is defined, independently of the value of β and the number of rings. These results show that the pattern formation is strongly modulated by the evaporation process.

Normalization in diffusion ϕ attenuates the effect of this phenomenon because it is defined as the ratio of diffusion coefficients of both species; which in fact are equal for particles of the same size (i.e., $\phi=1$). Dependence of patterns with diffusion coefficient can be investigated from the relationship, $\beta\gamma \sim 1/D_a^2$, which is valid when the geometrical (R, h), the density of solvent (ρ), and the multiplication of parameters J_0 (regarding strength evaporation) and κ (concerning precipitation) are constant. This relationship defines a set of hyperbolas in space β - γ cutting the contour curves as we can see in Fig. 7. The hyperbolas lie on a region depending on diffusion coefficient. This number depends, as before, on the values of β and γ , and it shows again the competition

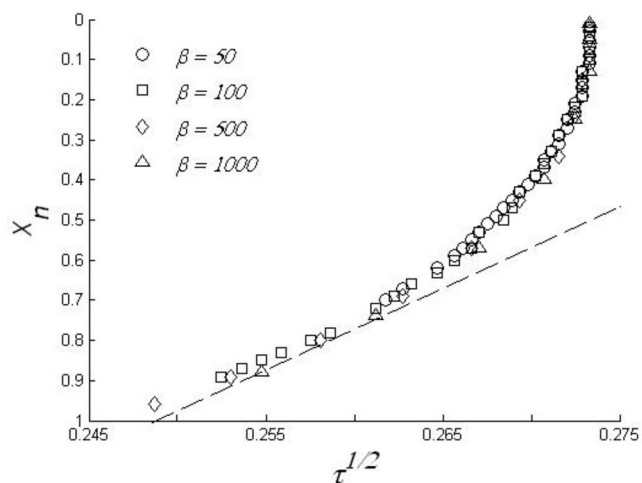


FIG. 11. A unique dynamic regime is established at different precipitation parameters with the evaporation parameter at $\gamma=1$.

between the precipitation and evaporation processes domain. Therefore, the diffusion process loses significance in pattern formation.

Now let us return to Fig. 2. Two patterns, one simulated numerically and the other obtained experimentally, were shown in Fig. 2. The experimental pattern shown [see Fig. 2(a)] is very well defined and has a good radial symmetry, with the exception of the center where disorder is observed. The simulation presented in Fig. 1(b) is very close to experimental results and it was only matched by the number of rings of the experimental pattern. The simulated rings are very well defined and represent a good approximation for the experimental result. The above results are obtained despite this model does not account explicitly for the interface forces that define the geometry and wetting of the drop, neither particle-particle nor particle-surface interactions. Although a more correct comparison of patterns in Fig. 2, our concern is to show how the competition between evaporation and precipitation is able to reproduce main characteristic of experimental results. Thus position, ratio of ring position, and width of the experimental and simulated rings are shown in Fig. 12. The simulated results reproduce main trends of experimental results and correspond to β and γ values close to $\beta=500$ and $\gamma=4$, respectively. Experimental results show a nonlinear decreasing for X_n which is followed by simulated ones, except near the center ($\xi=0$). This difference is a consequence of the presence of the disorder zone in the experiment which is not reproduced by the simulation. Ratio X_{n+1}/X_n shows a lightly decreasing behavior for the simulated results, with the exception at edge and center, which are discussed below, indicating an effect of confinement of species. Assuming a constant value of ratio X_{n+1}/X_n , a spacing coefficient p can be calculated providing the value of -0.091 ± 0.041 . The negative value of p comes from choice of origin of coordinates, but its absolute value lies in the usual range of Liesegang rings when n is large. This value may be associated to a mechanism of precipitation as in Liesegang rings [12]. Finally, W_n keeps practically a constant value for simulated results, with the exception to center and edge of drop. A constant value of W_n can be interpreted for

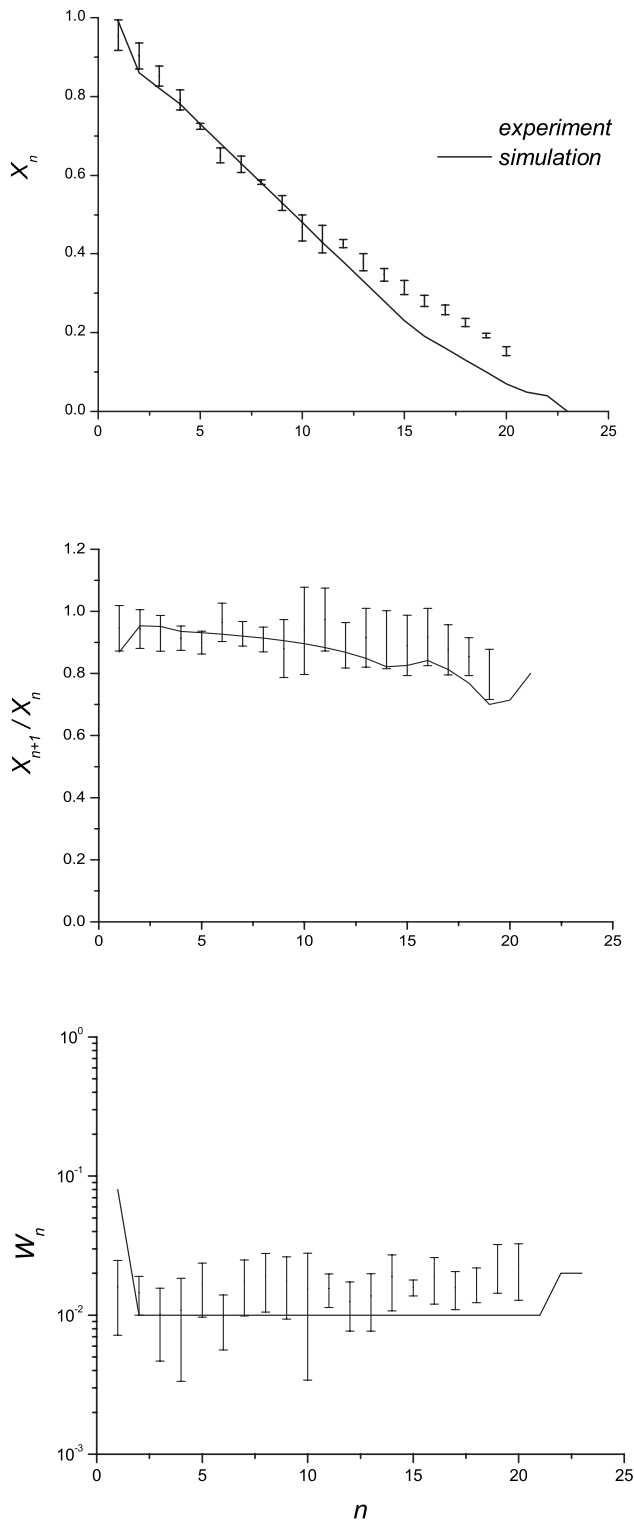


FIG. 12. Position, ratio of subsequent positions, and width of experimental (points with error bars) and simulated rings (solid line).

experimental results as indicating the presence of the selective process of precipitation. The selective process of precipitation can be related to properties of suspended particles (such as the size and the charge) and surface. In geometrical terms, precipitation occurs when contact angle is sufficiently small to trap particles in the edge of the drops [3], which

implies a selective process and therefore constant values for width of rings.

In comparison to experimental results [4], where X_{n+1}/X_n arrives to a constant for the last rings and W_n presents a maximum, in our case X_{n+1}/X_n presents the same, approximately constant, value and maximum for W_n is absent. A possible source of this last difference can be attributable to electrical charge of precipitates. In our case the precipitates are associations of positively and negatively charged particles with low effective electrical charge, while maximum of W_n has been observed for precipitation of positive particles on a negative surface, where electrical interaction is stronger. Also note that these behaviors are different than observed for Liesegang rings, where X_{n+1}/X_n arrives at a constant value only when n is large, and W_n is proportional to X_n . In our results, the former case occurs for any n while the latter behavior is not reproduced.

V. CONCLUDING REMARKS

We present results that reproduce symmetric rings from two precipitated species modulated by evaporation. In our results, two species are precipitated, without intermediate, following the theory of supersaturation while evaporation is assumed to be as in the evaporation of a liquid drop on a surface. The results are based on a numerical solution of a set of partial differential equations, where precipitation and evaporation are varied by the parameters β and γ , respectively. We show a monotonically decreasing of the ring position (X_n), as a function of n , which is a consequence of spatial constraint of ring formation. The ring formation begins at the boundary of a system and is limited by its center. With the exception to rings near boundary and center, we observe constant values for ratio X_{n+1}/X_n and a constant value for width of the rings (W_n). These trends are different to those followed by Liesegang rings, and define main tendencies of rings modulated by evaporation. This is confirmed by the spatiotemporal behavior observed in our approach. Additionally, precipitation parameter (β) defines different regimes for different γ values and the parameter (γ) only defines a regime for different values of β ; which is independent of the number of rings. Indeed, the number of rings is defined by competition between precipitation and evaporation processes; while diffusion is not relevant in formation of these structures. These results describe qualitatively well the pattern formation by precipitates of a mixture of positively and negatively charged particles. However, it should be noted that this approach does not account for surface tension or pinning effects along the contact line, and it is limited to a fixed boundary. An investigation in this direction is in progress by our group.

ACKNOWLEDGMENTS

This work was partially supported by Conacyt through Grants No. 49482, No. 180837 (G.L.), and No. 169393 (A.L-O.). One of the authors (E.P.) thanks E. Y. Sheu (Vanton Research Laboratory) for initial fruitful discussions.

- [1] R. D. Deegan, O. Bakajin, T. F. Dupont, G. Huber, S. R. Nagel, and T. A. Witten, *Nature (London)* **389**, 827 (1997).
- [2] R. D. Deegan, O. Bakajin, T. F. Dupont, G. Huber, S. R. Nagel, and T. A. Witten, *Phys. Rev. E* **62**, 756 (2000).
- [3] I. Karakurt, P. Leiderer, and J. Boneberg, *Langmuir* **22**, 2415 (2006).
- [4] M. A. Ray, H. Kim, and L. Jia, *Langmuir* **21**, 4786 (2005).
- [5] R. D. Deegan, *Phys. Rev. E* **61**, 475 (2000).
- [6] A. M. Turing, *Philos. Trans. R. Soc. London, Ser. B* **237**, 37 (1952).
- [7] R. B. Hoyle, *Pattern Formation: An Introduction to Methods*, 1st ed. (Cambridge University Press, Cambridge, 1996).
- [8] M. E. Le Van and J. Ross, *J. Phys. Chem.* **91**, 6300 (1987).
- [9] A. Toramaru, T. Harada, and T. Okamura, *Physica D* **183**, 133 (2003).
- [10] G. T. Dee, *Phys. Rev. Lett.* **57**, 275 (1986).
- [11] I. Lagzi, A. Volford, and A. Büki, *Chem. Phys. Lett.* **396**, 97 (2004).
- [12] T. Antal, M. Droz, J. Magnin, Z. Rácz, and M. Zrinyi, *J. Chem. Phys.* **109**, 9479 (1998).
- [13] A. Büki, É. Kárpáti-Smidróczki, and M. Zrinyi, *J. Chem. Phys.* **103**, 10387 (1995).
- [14] H.-J. Krug and H. Brandtstädter, *J. Phys. Chem. A* **103**, 7811 (1999).
- [15] M. Ripszám, A. Nagy, A. Volford, F. Izsák, and I. Lagzi, *Chem. Phys. Lett.* **414**, 384 (2005).
- [16] E. Adachi, A. S. Dimitrov, and K. Nagayama, *Langmuir* **11**, 1057 (1995).
- [17] L. Shmuylovich, Q. Shen, and H. A. Stone, *Langmuir* **18**, 3441 (2002).
- [18] M. Abkarian, J. Nunes, and H. A. Stone, *J. Am. Chem. Soc.* **126**, 5978 (2004).
- [19] Z. Lin and S. Granick, *J. Am. Chem. Soc.* **127**, 2816 (2005).
- [20] E. Rio, A. Daerr, F. Lequeux, and L. Limat, *Langmuir* **22**, 3186 (2006).
- [21] M. Ghosh, F. Fan, and K. J. Stebe, *Langmuir* **23**, 2180 (2007).
- [22] A. Kotara, K. Furusawa, Y. Takeda, and Z. Z. Kolloid, *Polymer* **239**, 677 (1970).
- [23] E. Martin and R. Shanahan, *Langmuir* **11**, 1041 (1995).
- [24] U. Ascher, S. Ruuth, and B. Wetton, *SIAM J. Numer. Anal.* **32**, 797 (1995).